Selection rules in the excitation of the divacancy and the nitrogen-vacancy pair in 4*H*- and 6*H*-SiC

Danial Shafizadeh,[1] Joel Davidsson,[1] Takeshi Ohshima,[2] Igor A. Abrikosov,[1] Nguyen T. Son,[1] and Ivan G. Ivanov[1,*]

[1]*Department of Physics, Chemistry and Biology, Linköping University, SE-58183, Linköping, Sweden*
[2]*National Institutes for Quantum Science and Technology, 1233 Watanuki, Takasaki, Gunma 370-1292, Japan; and Department of Materials Science, Tohoku University, 6-6-02 Aramaki-Aza, Aoba-ku, Sendai 980-8579, Japan*

(Received 16 November 2023; accepted 8 May 2024; published 3 June 2024)

In this study, we address selection rules with respect to the polarization of the optical excitation of two color centers in 4*H*-SiC and 6*H*-SiC with potential for applications in quantum technology, the divacancy and the nitrogen-vacancy pair. We show that the photoluminescence of the axial configurations of higher symmetry (C_{3v}) than the basal ones (C_{1h}) can be canceled using any excitation (resonant or nonresonant) with polarization parallel to the crystal axis ($E_L||c$). The polarization selection rules are determined using group-theoretical analysis and simple physical arguments showing that phonon-assisted absorption with $E_L||c$ is prohibited despite being formally allowed by group theory. A comparison with the selection rules for the silicon vacancy, another defect with C_{3v} symmetry, is also carried out. Using the selection rules, we demonstrate selective excitation of only one basal divacancy configuration in 4*H*-SiC, the PL3 line, and discuss the higher contrast and increased Debye-Waller factor in the selectively excited spectrum.

DOI: 10.1103/PhysRevB.109.235203

I. INTRODUCTION

Since the last few decades, the development of solid-state quantum bits (qubits) based on color centers in wide-band-gap semiconductors has been led by the negative nitrogen-vacancy (NV^-) centers in diamond, showing impressive progress in applications to nanoscale sensing and quantum communications [1,2]. However, no individual color center or material platform is ideal for all different applications. With time, more materials with specific advantages attract attention and join the race [3,4]. Among these, silicon carbide (SiC) is a promising one due to the fact that it hosts various color centers emitting light near and at telecom wavelengths with excellent optical and spin properties and, more importantly, for large-scale applications, it is the only wide-band-gap semiconductor that has industrial wafer-scale productions with well-controlled doping, mature complementary metal-oxide semiconductor (CMOS) technology, and established nanofabrication techniques [3–6].

Among various color centers in SiC, the negatively charged Si vacancy (V_{Si}^-, or simply V_{Si}) [7] and the neutral divacancy ($V_C V_{Si}^0$, or simply VV) [8], i.e., an uncharged complex of a Si vacancy (V_{Si}) and a nearest C vacancy (V_C), are the most studied. The divacancy spins have long coherence times, ranging from milliseconds in natural SiC [9] to several seconds in isotope-purified materials [10], and can be optically controlled at room temperature or even up to 550 K [11], making it suitable for broad temperature-range quantum sensing. Having emissions in the near-infrared spectral region around 1100 nm with a high-fidelity spin to photon interface [12] and good control of single nuclear spins [13], the neutral divacancy is also promising for quantum applications.

A defect that is analogous to the NV^- center in diamond is the negative N-vacancy center in SiC, i.e., the negatively charged complex between a N shallow donor at a C lattice site and a nearest Si vacancy ($N_C V_{Si}^-$, denoted hereafter as just NV) [14]. The center has an electronic structure analogical to that of the NV^- center in diamond but emits light near the *O* band of telecom wavelengths (∼1176−1243 nm) [15] which is more favorable for long-distance quantum communications.

The divacancy (VV) and NV centers have four and six different configurations in 4*H*- and 6*H*-SiC, respectively. In 4*H*-SiC (6*H*-SiC) there are two (three) axial configurations with C_{3v} symmetry, corresponding to the pairs with both constituents occupying the hexagonal sites (*hh*) or quasicubic sites (*kk* in 4*H*-SiC; k_1k_2 and k_2k_1 in 6*H*-SiC; here we use the notations of [16] for the lattice sites in 6*H*-SiC), and two (three) basal configurations with C_{1h} symmetry (*hk* and *kh* in 4*H*-SiC; hk_1, k_2k_2, and k_1h in 6*H*-SiC). Correspondingly, there are four zero-phonon lines (ZPLs) in 4*H*-SiC: PL1 (*hh*), PL2 (*kk*), PL3 (*hk*), and PL4 (*kh*) for VV [8]; NV1 (*hk*) NV2 (*kk*), NV3 (*hh*), and NV4 (*kh*) for NV^- [17]; and six ZPLs for both the VV and NV in 6*H*-SiC [16,18].

In nonresonant excitation experiments, the phonon-assisted absorption process is also involved. Since this process is also subject to selection rules, some defect configurations with a certain symmetry may not be excited. This is reflected in reported PL spectra, which often show ZPLs with very different intensities depending on the polarization of the

*ivaiv28@liu.se

excited laser [15,16,19]. Weak ZPLs excited with inappropriate polarization may appear in PL spectra of ensembles but can easily be missed in a scan for single emitters. Nonresonant excitation is a common way to activate and stabilize the bright charge state of color centers and is needed for obtaining their PL spectra. Identification of the selection rules for excitation including nonresonant excitation of ZPLs of defect centers with different symmetries is important for optimizing the PL detection or optically detected magnetic resonance (ODMR) of individual ZPLs. In this work, we investigate the selection rules in nonresonant excitation for the axial (C_{3v}) configurations of VV and NV centers in 4*H*- and 6*H*-SiC. We find a group-theoretical prediction (selection rule) which is opposed by physical arguments to yield a result opposite to that suggested by group theory. This finding implies that light with polarization parallel to the crystal axis is not absorbed by the axial configurations of VV and NV in both 4*H*- and 6*H*-SiC and, therefore, these configurations of the named defects are not excited. This observation provides us with a tool which distinguishes the axial from the basal configurations of these defects. Using this tool, we examine some published works which identify specific configurations, and suggest corrections to the published identifications. We also design an experiment with the divacancy ensemble in 4*H*-SiC in which only one divacancy configuration (PL3, *hk*) is excited, allowing us to obtain the pure ODMR signal of this configuration. Finally, we compare the selection rules in VV and NV with those for the silicon vacancy which also has C_{3v} symmetry.

II. EXPERIMENT

The samples used for the studies on the NV pairs are bulk N-doped (in the range of $10^{17}\,\mathrm{cm}^{-3}$) 4*H*- and 6*H*-SiC, irradiated and annealed to form NV pairs. The samples containing divacancies are either as-grown bulk high-purity semi-insulating (HPSI) materials, or electron irradiated to fluences in the 10^{17}–$10^{18}\,\mathrm{cm}^{-3}$ range HPSI bulk 4*H*- and 6*H*-SiC substrates, annealed to about 800 °C for 20–30 min to create divacancies. PL measurements are carried out using a Jobin Yvon HR460 monochromator equipped with 1200 and 300 grooves/mm (g/mm) gratings, and an InGaAs multichannel detector. The excitation laser is a tunable Ti-sapphire laser. Most spectra presented here are obtained with a laser at ∼930 nm unless stated otherwise. The samples are mounted in a variable temperature closed cycle cryostat and cooled down to 3.8 K. The resolution of ∼4 Å with the 300 g/mm grating is sufficient for most of the measurements, albeit a higher resolution of ∼1 Å has been needed using the 1200 g/mm for some closely spaced lines in 6*H*-SiC. A half-wave plate is placed in the path of the laser for rotating the polarization, and a polarizer is used in the emission path. The laser line is filtered using 1000 or 1100 nm long-pass filters. All measurements are done using a closed cycle cryostat (Montana Instruments Cryostation s50) at temperature ∼4 K.

III. THEORETICAL BACKGROUND

The polarization selection rules for the zero-phonon line (ZPL) emission, as derived from the symmetries of the ground and excited states and group-theoretical analysis, have been discussed for many color centers in previous works. For the divacancy and the V_{Si} such consideration can be found in Refs. [20,21], respectively. From a group-theoretical point of view, the selection rules for the divacancy and the NV center are the same because their ground and excited states have the same symmetry, and both defects have electronic spin $S = 1$. Furthermore, the same selection rules apply for resonant excitation in the ZPLs since the matrix elements for absorption into and emission in a ZPL are the same.

However, the selection rules for nonresonant excitation of a certain defect are rarely considered, and when there is such consideration, it is usually limited to experimental observations only (e.g., [22,23]). Nonresonant excitation refers to excitation at higher energy than the ZPL into the phonon sideband (PSB) of the defect. Hence it is phonon assisted with creation of a phonon in the absorption process, and one may assume that absorption will always be allowed if this phonon has a suitable symmetry. In this work, we refute this notion by showing that the phonon-assisted absorption into the excited state of some defects is also subject to strict selection rules. This may lead to configurations of the polarization of the exciting laser light with respect to the c axis for which the absorption from the ground to the excited state of the defect is strictly prohibited in the case of phonon-assisted transitions even though a formal group-theoretical analysis classifies it as allowed.

We examine here two different defects in the hexagonal 4*H*- and 6*H*-SiC polytypes: the neutral divacancy (VV^0, denoted shortly VV) and the negative nitrogen-vacancy pair (NV^-, or just NV), and compare with the silicon vacancy V_{Si} which has been treated elsewhere [18,23,24]. The presence of inequivalent lattice sites for Si and C, two in 4*H*-SiC and three in 6*H*-SiC, yields several defect centers (configurations) for the same type of defect. Thus the divacancy and the NV pair in 4*H*-SiC (6*H*-SiC) have four (six) inequivalent configurations, respectively. The silicon vacancy occupies either hexagonal or cubic Si sites, yielding two inequivalent configurations in 4*H*-SiC and three in 6*H*-SiC. All the above-mentioned defects have distinct ZPLs, and in some cases, the PL centers have been associated with specific configurations.

The configurations of VV and NV are further divided into axial and basal. The two (three) axial configurations possess C_{3v} symmetry, in 4*H*- (6*H*-) SiC, respectively. The remaining two (three) configurations in 4*H*- (6*H*-) SiC have lower symmetry, C_{1h}. Our study focuses on the high-symmetry (C_{3v}) axial configurations. The term "axial" reflects the fact that the orientation of the C_3 axis coincides with the crystal axis (c axis) along which the two constituents of the binary defects are aligned. We will show that the orientation of the exciting photon's polarization with respect to the c axis determines the probability for photon absorption, with this probability vanishing for polarization parallel to the c axis ($E||c$) in the case of both the divacancy and the NV pair in their axial configurations. However, the obtained selection rules are likely to be approximately valid also for the basal configurations with lower C_{1h} symmetry [25,26], but with different orientation of the polarization direction for which the absorption nearly vanishes. We underline that we consider here usual nonresonant excitation with photon energies above the energy

TABLE I. Selection rules for the divacancy and the NV pair in their axial configurations, and the silicon vacancy V_{Si} analyzed within the single C_{3v} group. A and F denote the allowed and forbidden transitions, respectively. The transition with $E||c$ assisted by phonons of E symmetry (denoted by A^*) is formally allowed by group theory but prohibited due to physical reasons discussed in the text.

NV pair or the divacancy (axial, C_{3v} symmetry): $^3A_2 \leftrightarrow {}^3E$ transition				
Polarization	Resonant excitation or ZPL	Phonon assisted (nonresonant) involving phonon of symmetry		
		A_1	A_2	E
$E\perp c$	A	A	A	A
$E\|\|c$	F	F	F	A^*
Silicon vacancy analyzed within C_{3v} symmetry: $^4A_2 \leftrightarrow {}^4A_2$ transition				
Polarization	Resonant excitation or ZPL	Phonon assisted (nonresonant) involving phonon of symmetry		
		A_1	A_2	E
$E\perp c$	F	F	F	A
$E\|\|c$	A	A	F	F

of the corresponding ZPL. The selection rules for resonant excitation into the ZPL are simpler and follow the selection rules for the photons emitted in the ZPL.

More details on the group-theoretical derivation of the selection rules are given in the Supplemental Material (SM) [27], covering both cases of resonant and nonresonant excitation. The results from the analysis are summarized in Table I for the three defects considered here, V_{Si}^-, and the axial configurations of $V_C V_{Si}^0$ and NV^-.

We notice that the latter two defects have common symmetry in 4H- and 6H-SiC (C_{3v}) and the same structure of the ground and excited states ($^3A_2$ and ^3E, respectively); hence their excitation is governed by the same selection rules. On the other hand, V_{Si} has the $^4A_2$ ground state in both polytypes. The excited state has two counterparts, $^4A_2$ and ^4E. In 4H-SiC, the $^4A_2$ is the lowest in energy excited state for both the cubic and hexagonal inequivalent vacancy configurations. The selection rules obtained within the single group C_{3v} for ZPL emission and resonant excitation are those between two $^4A_2$ quartets, yielding emission (or resonant excitation in the ZPL) allowed only with $E||c$ polarization. Another ZPL termed V1′ appears at higher energy as a companion of the V1 ZPL (associated with V_{Si} at the hexagonal site) at higher temperature, well visible above ∼5 K, stemming from the $^4E \leftrightarrow {}^4A_2$ transition. The selection rules derived within the single group C_{3v} predict $E\perp c$ polarization. We indicate, however, that the selection rules for V_{Si} derived within the single group are only approximate since a proper analysis should be carried out within the double group $\bar{C}_{3v}$ owing to the half-integer spin of the defect.

IV. RESULTS AND DISCUSSION

A. Emission selection rules

Although considered previously in different works, we summarize here and display in Table I the polarization selection rules for the ZPLs of the three defects considered here. We notice that the polarization of the ZPLs for the divacancy and the NV pair agree with the group-theoretical analysis (see Table I) and previous publications considering the specific cases of the divacancy in 4H-SiC [20] and the divacancies and NV pairs in 4H- and 6H-SiC [28]. According to the selection rules in C_{3v} symmetry, the polarization of the ZPLs of the axial configurations (PL1 and PL2 in 4H-SiC; QL1, QL2, and QL5 in 6H-SiC) is perpendicular to the axis of the vacancy pair, i.e., to the c axis ($E\perp c$).

B. Selection rules with respect to the polarization of nonresonant excitation

We use excitation at 930 nm from a continuous wave Ti-sapphire laser with linearly polarized emission. The polarization of the laser is rotated using a λ/2 plate which preserves the linear polarization for any rotation angle. The samples are mounted so that the c axis is in the focal plane of the objective or the collecting lens; hence the linear polarization of the incident laser can be chosen to conclude any angle with the c axis. In two cases, the NV pair in 4H-SiC and the divacancy in 6H-SiC, we had bulky samples with a parallelepiped shape allowing a weakly focused laser beam (by a lens of focal length ∼150 mm) on the sample and the use of a macroscopic collecting system consisting of a parabolic mirror and a 200 mm focal length lens for focusing on the monochromator slit. Sometimes with bulky samples we used also rectangular geometry: the **k** vector of the exciting beam is perpendicular to the c axis and to the detection direction. Thinner substrates (of thickness 350–500 μm) are mounted edge-on and a microscope objective is used to focus the laser on the edge of the sample and collect the emitted PL.

Figure 1 displays the spectra of the divacancy in 4H-SiC [Fig. 1(c)] and 6H-SiC [Fig. 1(d)] recorded with a polarization of the excitation laser E_L perpendicular and parallel to the c axis ($E_L\perp c$ and $E_L||c$, respectively). The most notable feature is the complete vanishing of half of the divacancy lines (in both 4H- and 6H-SiC) when excited with $E_L||c$ polarization. In complete analogy with the divacancy, half of the ZPLs associated with the NV pair vanish completely when the laser excitation applied to the sample has $E_L||c$ polarization. This is illustrated in Fig. 1 [panel (a) displays the spectra of 4H-SiC, and panel (b) in 6H-SiC]. The polar plots in Fig. 2 summarize the full angular dependence.

In both polytypes, half of the ZPLs for both considered defects correspond to the number of lines due to the axial

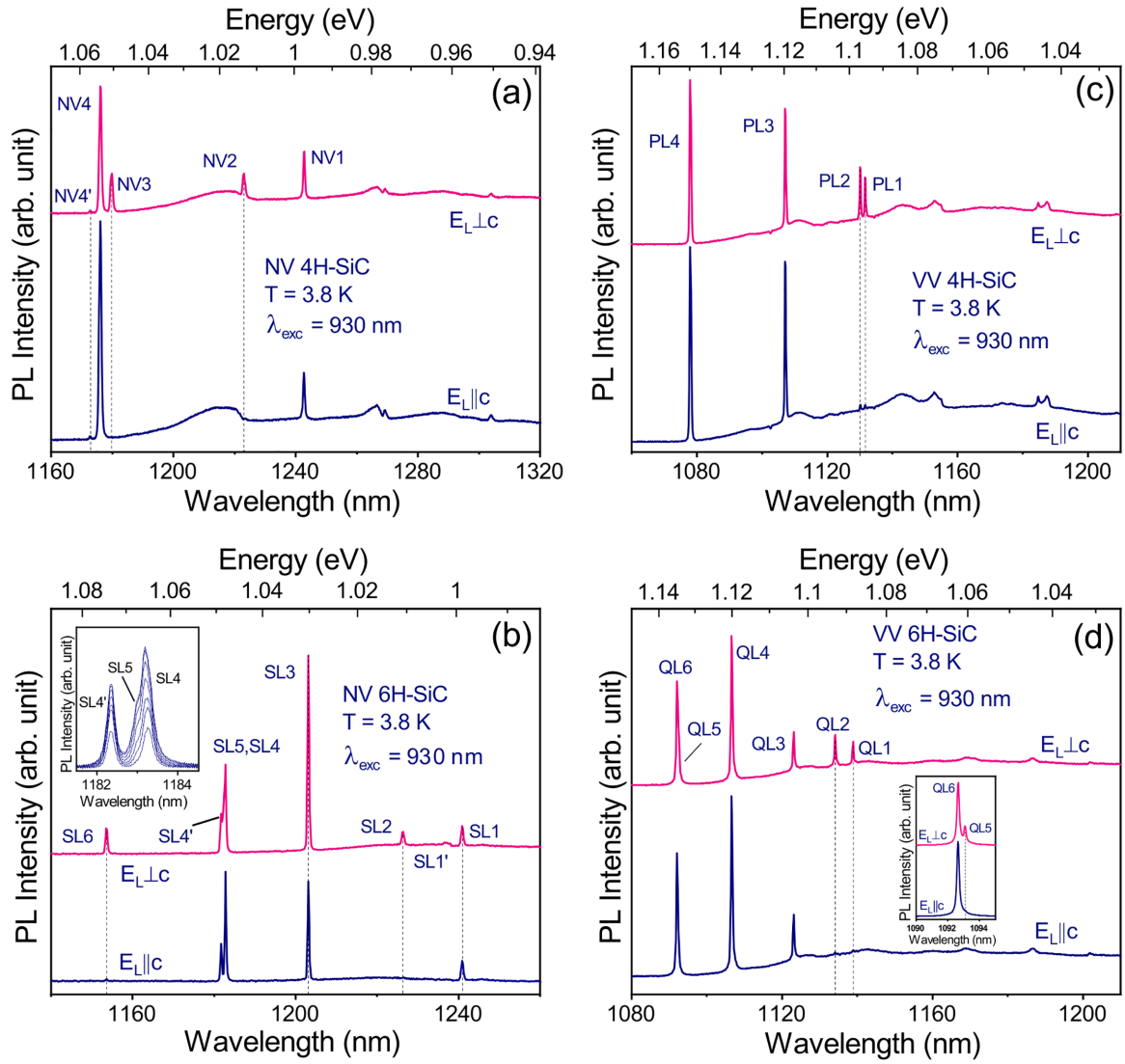

FIG. 1. Low-temperature PL spectra of the NV pair (a), (b) and the divacancy (c), (d) in 4H-SiC (a), (c) and 6H-SiC (b), (d). The ZPLs due to the axial configurations with C_{3v} symmetry all vanish for polarization of the excitation is $E_L||c$. The insets in (b), (d) show spectra recorded with higher resolution; the latter zooms in on the nearly degenerated QL5 and QL6 lines, while the former shows the angular dependence of the SL4 and SL5 lines recorded with 15 ° steps between $E_L\perp c$ (topmost curve) and $E_L||c$ (bottom curve). NV4′, SL1′, and SL4′ denote PL lines originating from closely spaced counterparts of the excited state detectable at temperatures ∼4 K. For the NV ZPLs in 6H-SiC we use the SL notations of Ref. [28] to avoid confusion with the NV lines in 4H-SiC.

configurations. We will show that the vanishing of lines with $E_L||c$ polarization identifies exactly these configurations and is a consequence of the C_{3v} symmetry and the symmetries of the ground (GS) and the excited (ES) states which are common for these two defects. Moreover, we will demonstrate that photons with $E_L||c$ polarization are not absorbed at all by the axial configurations; hence neither the ZPLs nor the associated phonon sidebands can appear in the spectra excited with $E_L||c$.

We refer to Table I, where the selection rules in C_{3v} symmetry for direct and phonon-assisted transition between the GS and the ES are listed. Since both defects (divacancy and NV) have integer spin ($S = 1$), the group-theoretical analysis is restricted to the single group C_{3v}. We see that the direct transitions for the axial configurations are forbidden with $E||c$ polarization and allowed with $E\perp c$ polarization, in agreement with theoretical analysis and experimental data for the divacancy in 4H-SiC [20] and our experimental data. Here E denotes the electric field polarization of the ZPLs; hence the same selection rules apply for *resonant* excitation ($E_L||c$ − forbidden, $E_L\perp c$ − allowed).

Let us consider now the phonon-assisted transitions for the axial configurations of the divacancy and the NV pair. There exist three possible symmetries for the phonons in C_{3v}, namely, A_1, A_2, and E. The former two symmetries are one dimensional, and the atomic displacements are along the c axis of the crystal, whereas the two-dimensional E representation of C_{3v} describes phonons with displacements in the basal plane, i.e., perpendicular to the c axis. Table I shows that all phonon-assisted transitions with $E\perp c$ polarization are allowed, whereas for $E||c$ only transitions assisted with phonons of E symmetry are allowed according to the formal

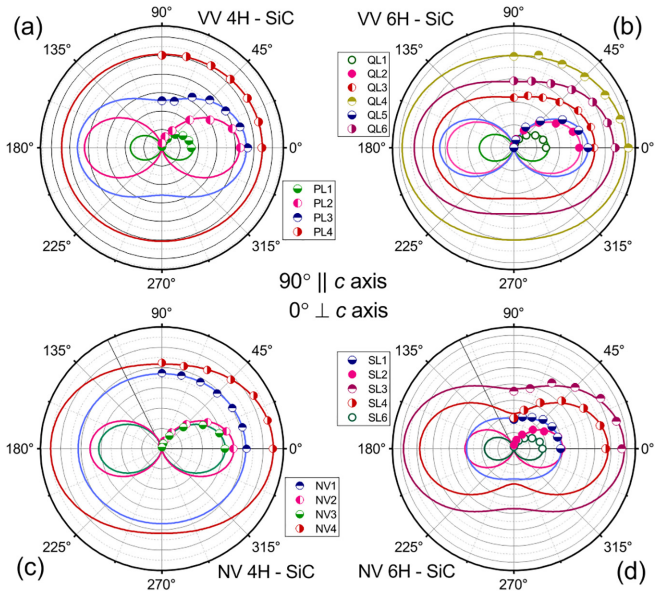

FIG. 2. Angular dependence of the ZPL intensity on the angle φ between the laser polarization and the c axis for the divacancy and the nitrogen-vacancy pair in 4H and 6H polytypes, as denoted for each polar plot. The experimental data are fitted with an expression of the form $I(\varphi) = A(1 + B\cos 2\varphi)$, where I is the ZPL intensity and A and B are fitting constants specific for each ZPL. $B = 1$ for the axial configurations. The laser polarization is $E_L \perp c$ at $\varphi = 0^\circ$ and $E_L || c$ at $\varphi = 90^\circ$.

group-theoretical analysis. However, light with $E||c$ polarization cannot interact with phonons of E symmetry because the electric field of the incident photons ($E||c$) is orthogonal to the atomic displacements of phonons with E symmetry. Consequently, such transitions are physically forbidden.

Since the considered defects have spin $S = 1$, we need to consider also whether the entailed spin orbit splitting of the E state (the ES) has an effect on the selection rules. In fact, the symmetry of the wave function is determined by the symmetry of its orbital part for wave functions with integer spin. Considering the double group (which is needed for analyzing selection rules for wave functions with half-integer spin), its use in the case of integer spin is redundant because the transformation properties of integer-spin wave functions under the extra symmetry operations of the double group are exactly the same as the transformation properties under the corresponding symmetry operations of the single group. The spin plays a role in the selection rules in the sense that only spin conserving optical transitions are allowed between the substates of the GS and the ES ([12]; see also the Supplemental Material [27]).

Thus we obtain that in the cases of the axial configurations of the divacancy and the NV pair in both 4H- and 6H-SiC, both direct and indirect (phonon-assisted) transitions with $E||c$ polarization are prohibited. When photon absorption is considered, i.e., the polarization E represents the polarization of the incident laser E_L, this means that absorption of photons by the axial configurations of the considered defects is prohibited for $E_L||c$ not only for the direct but also for the indirect (phonon-assisted) absorption, in complete agreement with the experimental data. Hence we have found a case of a transition with the selection rule which, if treated within group theory alone, predicts the unphysical result that this is an allowed transition. However, the transition is in fact forbidden by the physical argument that phonons with displacements perpendicular to the c axis cannot interact with light with $E_L||c$. This may not be the only exception when the group theory generates an unphysical result, which is interesting as a separate task going beyond the scope of the present paper.

We need to make a detour to address the weak appearance of the forbidden axial configurations PL1 and PL2 in the spectrum with $E_L||c$, e.g., in Fig. 1(c). For the rest of the figure, the samples used are bulk parallelepipeds with the c axis along one of the edges. Owing to the large dimensions of each face we can use a macroscopic lens for focusing the laser; hence $E_L||c$ can be implemented close to ideal, parallelly. In these cases, any contributions of the axial configurations with the $E_L||c$ are negligible [cf. panels (a), (b) in Fig. 1], in agreement with theory. We notice that even in this case the forbidden lines can "leak" into the spectrum if, for instance, the c axis is slightly out of the plane perpendicular to the **k** vector of the incident excitation, but such effect seems to be negligible for the bulk samples. On the other hand, the spectra in Fig. 1(c) are recorded with an on-edge mounted 350 μm thick substrate, which necessitates the use of a microscopic objective for excitation and light collection, to avoid penetration of the laser through the faces of the sample which would provide $E_L \perp c$ polarization. An objective with high numerical aperture (e.g., NA = 0.9) and strong focusing has an angle of incidence from zero up to ∼70 ° for the focused light. Hence, even if the polarization is aligned perfectly $E_L||c$ above the objective, after focusing some part of the excitation will be oriented at different angles with respect to the c axis. An estimate within the geometric optics approximation yields a contribution on the order of 1% from the perpendicular to the c-axis component of the laser polarization arising from the strong focusing by the objective [27]. This estimate is obtained assuming ideal alignment $E_L||c$ above the objective and c axis in the focal plane of the objective. Experimentally, we observe a contribution between 2.5% and up to 10% from the axial configurations in the PL spectra when using a microscope objective, even if the same sample is measured at different occasions. Also, with the bulk samples and using macro-optics for focusing and light collection we may see a contribution from the forbidden configurations if the c axis is not perfectly in the focal plane of the objective. Thus we attribute the weak appearance of the forbidden components in the experiment mainly to the nonideal alignment of the laser polarization with the c axis, and estimate that even if this alignment was ideal, we would still expect to see about 2%–3% from the maximum intensity (with $E_L \perp c$) of the lines forbidden with $E_L||c$ polarisation, if a microscope objective is used.

We now discuss the nonaxial configurations of the divacancy and NV, aka basal plane configurations, which have C_{1h} symmetry *per se*. The ground state has A'' symmetry compatible with the A_2 symmetry of the ground state in C_{3v}. (Here we denote the two irreducible representations of C_{1h} with A' and A'' to distinguish them from the A_1 and A_2 representations of C_{3v}.) The excited state of E symmetry splits into A' and A'' states when the symmetry is lowered to C_{1h}. Trivial

analysis shows that from a group-theoretical point of view, all transitions are allowed, i.e., with both $E||c$ and $E\perp c$ polarizations. In addition, for each of the basal configurations, there exist three equivalent orientations of the defect axis (the line connecting the two components of the defect). We notice that if $E||c$ polarization is considered, the polarization orientation is equivalent for all three orientations of a basal configuration. However, if an arbitrary $E\perp c$ polarization is considered, with photons propagating (nearly) along the c axis, as is the most common experimental geometry for both the impinging laser excitation and the received PL from the c face of a sample, the orientation of the polarization is different with respect to the axis of each of the three equivalent orientations. This has some interesting consequences, briefly discussed here in a qualitative manner.

C. Experimental implications

Let us consider first PL measurements on an ensemble of divacancies, or NV centers. In the usual backscattering-from-surface geometry of a c-plane sample with the c axis nearly perpendicular to the sample surface, the impinging photons propagate approximately along the c axis and, therefore, have perpendicular to c polarization ($E_L\perp c$). Whatever the orientation of this polarization with respect to the crystal axis, there will always be three equivalent angles between the axis of the defect and the laser polarization differing by 120 °. Thus, if we rotate the laser polarization in the basal plane, we do not expect any strong polarization dependence; i.e., PL intensity for the basal configuration will have more or less isotropic distribution with the angle of rotation of the polarization.

The situation is drastically different if PL measurements on single defects with basal configuration are considered, as studied in Ref. [22] for single NV pairs. If we rotate the polarization of the incident photons in the basal plane, there will be one direction in which the polarization is nearly parallel to the defect axis. Since the absorption for the axial configurations vanishes when the laser polarization is parallel to the c axis (i.e., to the defect axis), we may anticipate that also for the basal configurations the absorption will have a minimum when the laser polarization is parallel to the defect axis and maximum when it is perpendicular to it. Hence for a single defect we expect a strong dependence of the PL on the polarization orientation of the incident light for basal configurations, which has been observed in [22] for a single configuration of the NV pair in 4H-SiC at room temperature. The single defect with this property has been attributed to an axial configuration (the defect is labeled NV-15 in Ref. [22]), but in fact it should be attributed to one of the basal configurations. On the contrary, no strong dependence on the incident light polarization which would involve nearly vanishing of the PL for a certain incident light polarization is expected for the axial configurations (single defects or ensemble), because in the backscattering geometry considered here the laser polarization will be always perpendicular to the c axis ($E_L\perp c$) and the transition between the ground and excited state is always allowed. The defect labelled NV-1 in [22] has this property; the PL varies by a factor of 2 when the exciting laser polarization is rotated in the basal plane but does not vanish. Hence this defect should be associated with the axial configuration, not with the basal one as suggested in [22].

Using the notion that the axial configurations of VV and NV vanish when excited with $E_L||c$ as a tool for verifying the configuration, we can compare the experimental results presented in Fig. 1 with theoretical calculations. Theoretical data for the ZPLs of the NV center in 4H-SiC can be found in [15,17,29] and in 6H-SiC in [16]. The theoretical estimates for the ZPL positions of the divacancy are available in [30,31] and [18] for 4H- and 6H-SiC, respectively. The vanishing of the NV2 and NV3 lines when excited with $E_L||c$ implies that these two lines are associated with the axial hh and kk configurations in 4H-SiC [cf. Fig. 1(a)]. The theoretical calculations, however, yield that the lowest-energy ZPLs are associated with the axial configurations, indicating that the precision in the ZPL calculations is still insufficient for comparison with experiment [15,29]. Nevertheless, using the D-tensor parameters for identifications of the microscopic NV configurations correctly identifies the ZPL positions of the axial configurations [17]. In [16], the SL2, SL5, and SL6 lines are associated with the axial configurations in 6H-SiC, which is correct according to Fig. 1(b) (notice that Ref. [16] uses different notations for the ZPLs of the NV pair in 6H-SiC). For the divacancy, all theoretical calculations predict that the axial configurations have the lowest energy [30,31]. This is confirmed in Fig. 1(c) since PL1 and PL2 vanish for $E_L||c$ polarization. However, the assignment of the axial configurations for 6H-SiC in Ref. [18] needs adjustment, since the QL5 line identified in this reference as a basal configuration (hk_1) does vanish, while the QL6 line suggested to be axial configuration (k_2k_1) does not vanish for $E_L||c$ polarization. Since, according to Ref. [18], these two configurations have significant overlap of their Gaussian standard deviations (cf. Fig. 2(b) of Ref. [18]), indicating substantial probability that their ordering in energy is reversed compared to theory, it is most likely that the correct association of QL5 and QL6 is with the k_2k_1 and hk_1 configurations, respectively. We recall that here we use the notations of Refs. [16,32] for the hexagonal (h) and cubic (k_1, k_2) lattice sites in 6H-SiC (Ref. [18] uses somewhat different labeling of the lattice sites; hence hk_1 is hk_2 and k_2k_1 is k_2k_2 in Ref. [18]; the order is $V_{Si}V_C$). The corrected assignment for QL5 and QL6 is reflected in Table II.

The results are summarized in Table II for the two defects considered, VV and NV, in 4H- and 6H-SiC. In this table and in Figs. 1 and 2, we use the "SL" notations of Ref. [28] to denote the NV lines in 6H-SiC because of the following. Firstly, we do not use the "NV" notations of [16] to avoid confusion with the NV in 4H-SiC and, secondly, in [16] the lines are enumerated in order of ascending wavelength, whereas we prefer to enumerate all the lines for the divacancy and the nitrogen-vacancy pair in order of ascending energies.

D. Comparison with the silicon vacancy V_{Si}

It is instructive to compare the excitation selection rules for the axial divacancy and NV-pair configurations with those for the silicon vacancy V_{Si} which also possesses C_{3v} symmetry but has half-integer spin ($S = 3/2$). The GS and the ES of the latter defect are both quartets of A_2 symmetry, $^4A_2$. The selection rules deduced within the single group C_{3v} stipulate that

TABLE II. Summary of the line positions and their microscopic identification for the divacancy and the nitrogen-vacancy pair in 4*H*- and 6*H*-SiC. The nonresonant (phonon-assisted) excitation selection rules stipulate that $E_L||c$ polarization cannot excite all configurations denoted as axial. The basal configurations can be excited with both $E_L||c$ and $E_L\perp c$ polarization. The order of the sites is V_CV_{Si} for VV and N_CV_{Si} for NV. The notation for the lattice sites h, k_1, and k_2 for 6*H*-SiC follows Refs. [16,32] (different from Ref. [18]).

Line	Position in nm (meV)	Axial/basal	Identification
	Divacancy in 4*H*-SiC		
PL1	1132.0 (1095.0)	Axial	hh[a]
PL2	1130.5 (1096.5)	Axial	kk[a]
PL3	1107.6 (1119.1)	Basal	kh[a]
PL4	1078.5 (1149.3)	Basal	hk[a]
	Divacancy in 6*H*-SiC		
QL1	1139.6 (1087.6)	Axial	k_1k_2[b]
QL2	1135.0 (1092.1)	Axial	hh[b]
QL3	1123.9 (1102.9)	Basal	k_1h[b]
QL4	1107.4 (1119.3)	Basal	k_2k_2[b]
QL5	1093.5 (1133.5)	Axial	k_2k_1[b,c]
QL6	1093.0 (1134.0)	Basal	hk_1[b,c]
	Nitrogen-vacancy pair (NV^-) in 4*H*-SiC		
NV1	1242.7 (997.5)	Basal	hk[d]
NV2	1223.0 (1013.5)	Axial	kk[d]
NV3	1179.6 (1050.7)	Axial	hh[d]
NV4	1176.0 (1054.0)	Basal	kh[d]
	Nitrogen-vacancy pair (NV^-) in 6*H*-SiC		
SL1	1240.9 (998.9)	Basal	hk_1[e]
SL2	1226.4 (1010.7)	Axial	k_2k_1[e]
SL3	1203.1 (1030.2)	Basal	k_2k_2[e]
SL4	1182.9 (1047.8)	Basal	k_1h[e]
SL5	1182.6 (1048.1)	Axial	hh[e]
SL6	1153.7 (1074.3)	Axial	k_1k_2[e]

[a]From Refs. [9,23]. Note that [9] uses the order V_CV_{Si} for labeling.
[b]From Ref. [18].
[c]The QL5 and QL6 lines are reassigned in this work, as explained in the text.
[d]According to Ref. [33].
[e]From Ref. [16].

transitions with $E\perp c$ are forbidden for the ZPLs of both configurations, hexagonal and cubic, while the $E||c$ transitions are allowed [21,23]. This is also what is approximately observed experimentally (see [23,27]), albeit most experiments can register a weak contribution from the "forbidden" perpendicular to the c-axis polarization. However, the notion that the single-group selection rules are approximately valid also in the description of the silicon vacancy might be misleading, because a proper treatment of the selection rules must be done within the double group $\bar{C}_{3v}$. In fact, we will show below that the observed dominating polarization of the V1 and V2 lines in 4*H*-SiC is likely associated with the well-known spin polarization of V_{Si} under optical excitation and not with the "approximate validity of the single-group selection rules". In the case of half-integer spin, all substates of the ground and excited states transform as one of the extra representations of the double group, $E_{1/2}$, $^1E_{3/2}$, or $^2E_{3/2}$ [34]. The former two-dimensional representation describes the transformation properties of a wave function with spin component $S_z = \pm 1/2$, and the latter two one-dimensional representations are subject to time-reversal (Kramer's) degeneracy and their direct sum $E_{3/2} = {}^1E_{3/2} \oplus {}^2E_{3/2}$ represents the transformation properties of the wave functions with $S_z = \pm 3/2$. The selection rules for the ZPL (direct transitions) can be expressed with the following three statements (see, e.g., [35]):

$$E_{1/2} \leftrightarrow E_{1/2}, \quad \text{allowed with } E||c \text{ and } E\perp c, \tag{1a}$$

$$E_{1/2} \leftrightarrow E_{3/2}, \quad \text{allowed with } E\perp c, \text{ and} \tag{1b}$$

$$E_{3/2} \leftrightarrow E_{3/2}, \quad \text{allowed with } E||c. \tag{1c}$$

Here E denotes the emitted photon polarization if ZPL emission is considered, or $E \equiv E_L$ if resonant absorption is considered. The selection rules for phonon-assisted absorption remain unchanged for $E_L||c$ (only phonons of A_1 and A_2 symmetry can assist the absorption process). On the other hand, phonon-assisted absorption with $E_L\perp c$ can only involve phonons of E symmetry, and in this case all phonon-assisted transitions are allowed ($E_{1/2} \leftrightarrow E_{1/2}$, $E_{1/2} \leftrightarrow E_{3/2}$, and $E_{3/2} \leftrightarrow E_{3/2}$). Notice that both quartets, $^4A_2$ (GS) and $^4A_2$ (ES), contain both substates, $S_z = \pm 1/2$ transforming as $E_{1/2}$, and $S_z = \pm 3/2$ transforming as $E_{3/2}$. Since the zero-field splitting (ZFS) between the substates comprising the GS and the ES is in the tens of MHz range, it is unresolvable in optical experiments and in the ZPLs we expect to see a contribution from both polarizations, $E\perp c$ and $E||c$.

Nevertheless, both V1 and V2 manifest dominating $E||c$ polarization which may be due to the polarization of the ground (and, possibly, excited) states under optical excitation. It has been shown that the $E_{3/2}$ sublevel of the GS has dominant population (above 90% [36]) under optical excitation [37]. The same dominant population of the $E_{3/2}$ sublevel of the ES can be anticipated, because if the $E_{1/2}$ sublevel of the ES also had substantial population one would expect to see a significant contribution in the ZPL from $E\perp c$ polarization from recombination from $E_{1/2}$ to both counterparts $E_{1/2}$ and $E_{3/2}$, in accord with Eqs. (1a) and (1b). Such contribution is present but nearly negligible, compared to the $E||c$ component of the ZPLs V1 and V2 [27]. Thus, if both the GS and the ES have predominantly radiative recombination with $E||c$, it is the recombination between the two $E_{3/2}$ counterparts of the ES and GS. A similar hypothesis can be stated for the V1′ line. If the ES in this transition has a dominant $E_{1/2}$ population, and the recombination to $E_{3/2}$ has a larger probability than that of $E_{1/2}$, then we can understand the observed dominant $E\perp c$ polarization in the V1′ line. However, for the moment the only experimental evidence in favor of this hypothesis is that the final state in most of the radiative transitions is $E_{3/2}$, as demonstrated by the spin polarization [36]. Further theoretical work is needed to investigate the probabilities for population of the sublevels in the ES, for both $^4A_2$ and ^4E; hence the provided possible explanation of the ZPLs' polarizations should be considered hypothetical for the moment.

Experimental data illustrating the presence of $E\perp c$ polarization in the V1 and V2 lines and the weak $E||c$ component in the V1′ line are given in [27].

E. Selective excitation of the PL3 line of the divacancy in 4*H*-SiC

Low-temperature PL measurements on a divacancy ensemble in 4*H*-SiC without special regard for the polarization of the exciting laser usually display all four ZPL lines PL1–PL4 if the laser energy is higher than the energy of PL4 (the highest-energy ZPL). As discussed earlier, if excitation with $E_L||c$ polarization is used the axial configurations with ZPLs PL1 and PL2 together with their pertaining phonon sidebands (PSBs) are not excited at all. If, in addition, the laser energy is chosen between the energy positions of PL3 and PL4, then only the PL3 line will be excited. Thus a single ZPL together with its PSB for the divacancy in 4*H*-SiC can be isolated in the PL spectrum of divacancies ensemble containing all configurations. The situation is like that of observation of the PL from a single defect (in this case, PL3 corresponding to the *hk* configuration of $V_{Si}V_C$ in 4*H*-SiC), but with the benefit of the much stronger signal associated with the ensemble.

This selective excitation of the PL3 line in an ensemble is depicted in Fig. 3(a). The upper spectrum is obtained with excitation at 1090 nm (1.1371 eV) in between the PL4 (1.1493 eV) and PL3 (1.1191 eV) lines. The laser is filtered using two sharp-edge long-pass filters with a cutoff at 1100 nm. The bottom spectrum obtained with the common excitation of 930 nm (1.333 eV) above the energy of all four ZPLs is given for comparison. Figure 3(b) shows two ODMR spectra obtained with the same microwave antenna configuration but different excitation wavelengths, nonselective excitation with the laser at 1020 nm (lighter thicker curve) and selective excitation with 1090 nm (darker thinner curve). In both cases $E_L||c$ is used, so that the former ODMR spectrum contains a contribution from only PL3 and PL4 (PL1 and PL2 are not excited), while the ODMR spectrum with selective excitation contains the pure PL3 contribution corresponding to the top spectrum displayed in Fig. 3(a). We point out two features of the experiment with selective excitation of PL3. Firstly, the ODMR contrast is improved by at least a factor of 2 as seen from Fig. 3(b), which is anticipated because the background contribution from PL4 and its phonon sideband to the ODMR signal of PL3 is removed. The use of excitation with E_L not parallel to the c axis will further deteriorate the contrast due to the added contribution from PL1 and PL2 to the background. The second feature concerns the Debye-Waller (DW) factor of the PL3 line which shows a significant increase compared to the spectrum obtained with common excitation at 930 nm. The origin of this improvement is not understood at present and a thorough investigation of the factors influencing the DW factor is beyond the scope of this work. Nevertheless, the possibility of dealing with a single selectively excited ZPL with intensity typical for an ensemble may prove beneficial in future sensor applications.

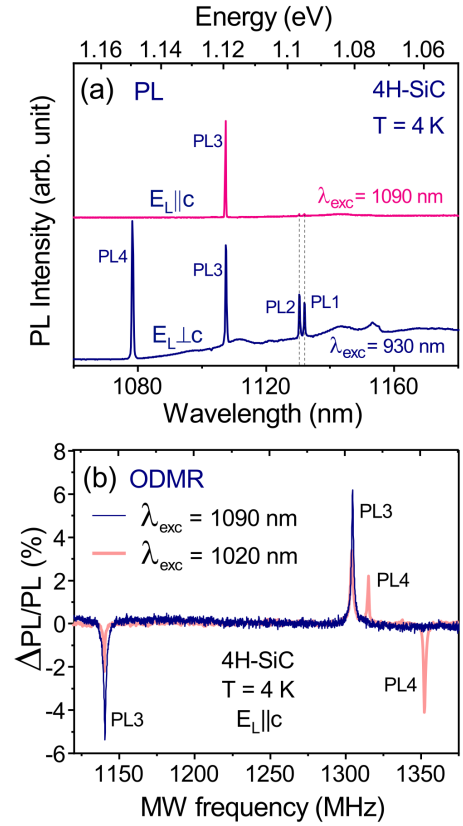

FIG. 3. Selective excitation of the PL3 line in ensemble of divacancies in 4*H*-SiC. (a) Selectively excited spectrum of PL3 line (top curve) using excitation with $E_L||c$ polarization and energy lower than the PL4 line (laser at 1090 nm, or 1.137 eV). PL1 and PL2 are not excited because there is no absorption for these configurations with $E_L||c$ polarization. The bottom spectrum showing all four divacancy lines and their phonon sidebands is provided for comparison (excitation with $E_L \perp c$ at 930 nm). Note the enhanced Debye-Waller factor with selective excitation of PL3. (b) ODMR spectra obtained using the selective excitation of PL3 only (dark thinner curve) and of PL3 and PL4 using higher laser energy (light thicker curve), illustrating the contrast improvement for PL3 when the background emission of PL4 is removed, as discussed in the text.

V. SUMMARY

In conclusion, we have demonstrated theoretically and experimentally that the high-symmetry (axial) configurations of the divacancy and the NV pair in both 4*H*- and 6*H*-SiC are highly sensitive to the polarization of the exciting laser. No absorption and hence no excitation of the axial configurations occurs if the polarization of the excitation is $E_L||c$. This is shown to be due to the fact that only phonons of E symmetry may participate in allowed transitions between the ground and excited states for $E_L||c$, according to the group-theoretical selection rules. However, phonons with in-plane displacements cannot interact with photons of $E_L||c$ polarization since the electric field of the electromagnetic wave is orthogonal to the displacement of phonons of E symmetry. A comparison with the properties of the silicon vacancy V_{Si} which also has a GS of orbital A_2 symmetry and an ES of E symmetry for some configurations, but possesses half-integer spin, shows that excitation of the corresponding configurations ($A_2 \leftrightarrow E$ transition corresponds to the V1′ line) is not prohibited. This is attributed to the necessity of analyzing the selection rules within the double group $\bar{C}_{3v}$. The energy ordering of the divacancy ZPLs in 4*H*-SiC allows selective excitation of only one of the four configurations (PL3 line) using suitable laser

energy and $E_L||c$ polarization which can be useful for using the PL3 line in sensor applications with an ensemble of divacancies.

ACKNOWLEDGMENTS

Financial support from the Knut and Alice Wallenberg Foundation (Grant No. KAW 2018.0071) and the EU H2020 Project QuanTELCO (Grant No. 862721) is acknowledged. D.S. acknowledges support from the AFM (CeNano Grant No. 2021). J.D. acknowledges support from the Swedish e-science Research Centre (SeRC) and the Swedish Research Council (VR) Grant No. 2022-00276. T.O. expresses thanks for the support from the Japan Society for the Promotion of Science JSPS KAKENHI (Grants No. 20H00355 and No. 21H04553).

[1] M. H. Abobeih, J. Randall, C. E. Bradley, H. P. Bartling, M. A. Bakker, M. J. Degen, M. Markham, D. J. Twitchen, and T. H. Taminiau, Atomic-scale imaging of a 27-nuclear-spin cluster using a quantum sensor, Nature (London) **576**, 411 (2019).

[2] M. Ruf, N. H. Wan, H. Choi, D. Englund, and R. Hanson, Quantum networks based on color centers in diamond, J. Appl. Phys. **130**, 070901 (2021).

[3] M. Atatüre, D. Englund, N. Vamivakas, S.-Y. Lee, and J. Wrachtrup, Material platforms for spin-based photonic quantum technologies, Nat. Rev. Mater. **3**, 38 (2018).

[4] D. D. Awschalom, R. Hanson, J. Wrachtrup, and B. B. Zhou, Quantum technologies with optically interfaced solid-state spins, Nat. Photonics **12**, 516 (2018).

[5] A. Lohrmann, B. C. Johnson, J. C. McCallum, and S. Castelletto, A review on single photon sources in silicon carbide, Rep. Prog. Phys. **80**, 034502 (2017).

[6] N. T. Son, C. P. Anderson, A. Bourassa, K. C. Miao, C. Babin, M. Widmann, M. Niethammer, J. Ul Hassan, N. Morioka, I. G. Ivanov, F. Kaiser, J. Wrachtrup, and D. D. Awschalom, Developing silicon carbide for quantum spintronics, Appl. Phys. Lett. **116**, 190501 (2020).

[7] E. Sörman, N. T. Son, W. M. Chen, O. Kordina, C. Hallin, and E. Janzén, Silicon vacancy related defect in 4*H* and 6*H* SiC, Phys. Rev. B **61**, 2613 (2000).

[8] W. F. Koehl, B. B. Buckley, F. J. Heremans, G. Calusine, and D. D. Awschalom, Room temperature coherent control of defect spin qubits in silicon carbide, Nature (London) **479**, 84 (2011).

[9] D. J. Christle, A. L. Falk, P. Andrich, P. V Klimov, J. U. Hassan, N. T. Son, E. Janzén, T. Ohshima, and D. D. Awschalom, Isolated electron spins in silicon carbide with millisecond coherence times, Nat. Mater. **14**, 160 (2015).

[10] C. P. Anderson, E. O. Glen, C. Zeledon, A. Bourassa, Y. Jin, Y. Zhu, C. Vorwerk, A. L. Crook, H. Abe, J. Ul-Hassan, T. Ohshima, N. T. Son, G. Galli, and D. D. Awschalom, Five-second coherence of a single spin with single-shot readout in silicon carbide, Sci. Adv. **8**, eabm5912 (2022).

[11] F.-F. Yan, J.-F. Wang, Q. Li, Z.-D. Cheng, J.-M. Cui, W.-Z. Liu, J.-S. Xu, C.-F. Li, and G.-C. Guo, Coherent control of defect spins in silicon carbide above 550 K, Phys. Rev. Appl. **10**, 044042 (2018).

[12] D. J. Christle, P. V. Klimov, C. F. de las Casas, K. Szász, V. Ivády, V. Jokubavicius, J. Ul Hassan, M. Syväjärvi, W. F. Koehl, T. Ohshima, N. T. Son, E. Janzén, A. Gali, and D. D. Awschalom, Isolated spin qubits in SiC with a high-fidelity infrared spin-to-photon interface, Phys. Rev. X **7**, 021046 (2017).

[13] A. Bourassa, C. P. Anderson, K. C. Miao, M. Onizhuk, H. Ma, A. L. Crook, H. Abe, J. Ul-Hassan, T. Ohshima, N. T. Son, G. Galli, and D. D. Awschalom, Entanglement and control of single nuclear spins in isotopically engineered silicon carbide, Nat. Mater. **19**, 1319 (2020).

[14] H. J. von Bardeleben, J. L. Cantin, E. Rauls, and U. Gerstmann, Identification and magneto-optical properties of the NV center in 4*H*-SiC, Phys. Rev. B **92**, 064104 (2015).

[15] S. A. Zargaleh, B. Eble, S. Hameau, J.-L. Cantin, L. Legrand, M. Bernard, F. Margaillan, J.-S. Lauret, J.-F. Roch, H. J. von Bardeleben, E. Rauls, U. Gerstmann, and F. Treussart, Evidence for near-infrared photoluminescence of nitrogen vacancy centers in 4*H*-SiC, Phys. Rev. B **94**, 060102(R) (2016).

[16] Kh. Khazen, H. J. von Bardeleben, S. A. Zargaleh, J. L. Cantin, M. Zhao, W. Gao, T. Biktagirov, and U. Gerstmann, High-resolution resonant excitation of NV centers in 6*H*-SiC: A matrix for quantum technology applications, Phys. Rev. B **100**, 205202 (2019).

[17] S. A. Zargaleh, H. J. von Bardeleben, J. L. Cantin, U. Gerstmann, S. Hameau, B. Eblé, and W. Gao, Electron paramagnetic resonance tagged high-resolution excitation spectroscopy of NV-centers in 4*H*-SiC, Phys. Rev. B **98**, 214113 (2018).

[18] J. Davidsson, V. Ivády, R. Armiento, T. Ohshima, N. T. Son, A. Gali, and I. A. Abrikosov, Identification of divacancy and silicon vacancy qubits in 6*H*-SiC, Appl. Phys. Lett. **114**, 112107 (2019).

[19] B. Magnusson, N. T. Son, A. Csore, A. Gällström, T. Ohshima, A. Gali, and I. G. Ivanov, Excitation properties of the divacancy in SiC, Phys. Rev. B **98**, 195202 (2018).

[20] J. Davidsson, Theoretical polarization of zero phonon lines in point defects, J. Phys.: Condens. Matter **32**, 385502 (2020).

[21] E. Janzén, A. Gali, P. Carlsson, A. Gällström, B. Magnusson, and N. T. Son, The silicon vacancy in SiC, Physica B (Amsterdam) **404**, 4354 (2009).

[22] J.-F. Wang, Zh.-H. Liu, F.-F. Yan, Q. Li, X.-G. Yang, L. Guo, X. Zhou, W. Huang, J.-S. Xu, C.-F. Li, and G.-C. Guo, Experimental optical properties of single nitrogen vacancy centers in silicon carbide at room temperature, ACS Photonics **7**, 1611 (2020).

[23] I. D. Breev, Z. Shang, A. V. Poshakinskiy, H. Singh, Y. Berencén, M. Hollenbach, S. S. Nagalyuk, E. N. Mokhov, R. A. Babunts, P. G. Baranov, D. Suter, S. A. Tarasenko, G. V. Astakhov, and A. N. Anisimov, Inverted fine structure of a 6*H*-SiC qubit enabling robust spin-photon interface, npj Quantum Inf. **23**, 1 (2022).

[24] V. Ivády, J. Davidsson, N. T. Son, T. Ohshima, I. A. Abrikosov, and A. Gali, Identification of Si-vacancy related room-temperature qubits in 4*H* silicon carbide, Phys. Rev. B **96**, 161114(R) (2017).

[25] K. C. Miao, A. Bourassa, C. P. Anderson, S. J. Whiteley, A. L. Crook, S. L. Bayliss, G. Wolfowicz, G. Thiering, P. Udvarhelyi, V. Ivády, H. Abe, T. Ohshima, Á. Gali, and D. D. Awschalom, Electrically driven optical interferometry with spins in silicon carbide, Sci. Adv. **5**, eaay0527 (2019).

[26] Q. Li, J.-F. Wang, F.-F. Yan, J.-Y. Zhou, H.-F. Wang, H. Liu, L.-P. Guo, X. Zhou, A. Gali, Z.-H. Liu, Z.-Q. Wang, K. Sun, G.-P. Guo, J.-S. Tang, H. Li, L.-X. You, J.-S. Xu, C.-F. Li, and G.-C. Guo, Room-temperature coherent manipulation of single-spin qubits in silicon carbide with a high readout contrast, Natl. Sci. Rev. **9**, nwab122 (2022).

[27] See Supplemental Material at http://link.aps.org/supplemental/10.1103/PhysRevB.109.235203 for further details on the selection rules, discussion of the selection rules in the double group C_{3v} for the case of half-integer defect spin of the silicon vacancy, and influence of the nonideal experimental conditions on the spectra recorded with $E_L||c$.

[28] A. Gällström, Optical characterization of deep level defects in SiC, Ph.D. thesis, Dissertation No. 1674, Linköping University, 2015.

[29] A. Csóré, H. J. von Bardeleben, J. L. Cantin, and A. Gali, Characterization and formation of NV centers in 3*C*, 4*H*, and 6*H* SiC: An *ab initio* study, Phys. Rev. B **96**, 085204 (2017).

[30] L. Gordon, A. Janotti, and C. G. Van de Walle, Defects as qubits in 3*C*- and 4*H*-SiC, Phys. Rev. B **92**, 045208 (2015).

[31] J. Davidsson, V. Ivády, R. Armiento, N. T. Son, A. Gali, and I. A. Abrikosov, First principles predictions of magneto-optical data for semiconductor point defect identification: The case of divacancy defects in 4*H*−SiC, New J. Phys. **20**, 023035 (2018).

[32] H. J. von Bardeleben, J. L. Cantin, A. Csóré, A. Gali, E. Rauls, and U. Gerstmann, NV centers in 3*C*, 4*H*, and 6*H* silicon carbide: A variable platform for solid-state qubits and nanosensors, Phys. Rev. B **94**, 121202(R) (2016).

[33] Z. Mu, S. A. Zargaleh, H. J. von Bardeleben, J. E. Fröch, M. Nonahal, H. Cai, X. Yang, J. Yang, X. Li, I. Aharonovich, and W. Gao, Coherent manipulation with resonant excitation and single emitter creation of nitrogen vacancy centers in 4*H* silicon carbide, Nano Lett. **20**, 6142 (2020).

[34] R. Nagy, M. Widmann, M. Niethammer, D. B. R. Dasari, I. Gerhardt, Ö. O. Soykal, M. Radulaski, T. Ohshima, J. Vuckovic, N. T. Son, I. G. Ivanov, S. E. Economou, C. Bonato, S.-Y. Lee, and J. Wrachtrup, Quantum properties of dichroic silicon vacancies in silicon carbide, Phys. Rev. Appl. **9**, 034022 (2018).

[35] B. Kaufmann, A. Dörnen, and F. S. Ham, Crystal-field model of vanadium in 6*H* silicon carbide, Phys. Rev. B **55**, 13009 (1997).

[36] V. A. Soltamov, A. A. Soltamova, P. G. Baranov, and I. I. Proskuryakov, Room temperature coherent spin alignment of silicon vacancies in 4*H*- and 6*H*-SiC, Phys. Rev. Lett. **108**, 226402 (2012).

[37] Ö. O. Soykal, P. Dev, and S. E. Economou, Silicon vacancy center in 4*H*-SiC: Electronic structure and spin-photon interfaces, Phys. Rev. B **93**, 081207(R) (2016).